Identification of jarosite and other major mineral Fe phases in acidic environments affected by mining-metallurgy using X-ray Absorption Spectroscopy: With special emphasis on the August 2014 Cananea acid spill

Ingrid Nayeli Escobar-Quiroz[1,3,*], Mario Villalobos-Peñalosa[1], Teresa Pi-Puig[1], Francisco Martín Romero[1], and Javier Aguilar-Carrillo de Albornoz[2]

[1] *Instituto de Geología y Laboratorio Nacional de Geoquímica y Mineralogía (LANGEM), Universidad Nacional Autónoma de México, C.P. 04510, Ciudad de México, Mexico.*
[2] *Departamento de Tecnología Ambiental, Instituto de Metalurgia, Universidad Autónoma de San Luis Potosí (UASLP), Av. Sierra Leona 550, Lomas 2da sección, C.P. 78210, San Luis Potosí, S.L.P., Mexico.*
[3] *Posgrado en Ciencias de la Tierra, Universidad Nacional Autónoma de México (UNAM), Unidad de Posgrado, edificio D, primer piso. Cd. Universitaria, Coyoacán, C.P. 04510, Ciudad de México, Mexico.*
**chiprecart@yahoo.com.mx*

ABSTRACT

The sulfuric acid spill into the Sonora river, enriched in iron and copper ions from the Buenavista del Cobre mine (Cananea), gave way to the formation of various solid iron (Fe) phases. In this study, the mineral phases were identified by X-ray Absorption Spectroscopy (XAS) and bulk powder X-Ray Diffraction (XRD), and chemically through acid digestions for multielemental quantification, as well as a 3-step selective sequential extraction (SSE) to quantify the types of Fe oxide phases and the contribution of the associated elements. Jarosite was the only Fe mineral identified by XRD, but XAS allowed identification of jarosite with potentially toxic elements (PTEs) incorporated in its structure, making these elements less prone to leaching. In addition, very poorly crystalline phases such as schwertmannite and ferrihydrite were identified in several samples through XAS, which was confirmed by SSE. These phases are probably associated with PTEs. Other possible adsorbent Fe(III) minerals were also identified by XAS, such as maghemite and goethite; as well as mixed Fe(II)-Fe(III) minerals, such as green rust. It was possible to infer the influence of the acid spill on the different sampled areas through various Fe phases identified and/or the presence of gypsum. The influence was detected to be lower where the mineralogy was not associated to low pH and high sulfate concentrations. All precipitated Fe(III) phases downriver from the acid spill are known for their high retention capacities of PTEs either from incorporation into their structures and/or from surface adsorption, thus, contributing to the immobilization of the initial metal(loid) pollution caused by the acid spill. In addition, several other samples of mining-metallurgical wastes were analyzed by the same three techniques, suggesting many of the findings from the secondary Fe mineralogy of the Buenavista del Cobre mine acid spill as common processes occurring in mining-affected environments.

Key words: Fe phases; X-ray Absorption Spectroscopy (XAS); Geochemistry; Cananea; acid spill; Mexico.

RESUMEN

El derrame de ácido sulfúrico enriquecido en iones de cobre y hierro proveniente de la mina Buenavista del Cobre *(Cananea), sobre el río Sonora, dio paso a la formación de varias fases sólidas de hierro (Fe). En el presente estudio, estas fases fueron identificadas mediante análisis mineralógicos de Espectroscopía de Absorción de Rayos-X (XAS por sus siglas en inglés) y Difracción de Rayos-X (DRX), y químicamente por medio de una digestión ácida con cuantificación multielemental, así como extracciones secuenciales selectivas (ESS) de tres pasos para cuantificar los tipos de fases de óxido de Fe y la contribución de ciertos elementos asociados a dichas fases. La jarosita fue el único mineral de Fe identificado por DRX. Sin embargo, por XAS se observó que la jarosita contiene elementos potencialmente tóxicos (EPTs) incorporados en su estructura, siendo de esta forma menos lixiviables. Además, se logró identificar por XAS a los minerales poco cristalinos schwertmannita y ferrihidrita en varias de las muestras, corroborado por las ESS, donde se observa su posible asociación con EPTs. Otros minerales de Fe(III) posiblemente adsorbentes se identificaron también por XAS, como la maghemita y la goethita, además de minerales mixtos de Fe(II)-Fe(III), como el "green rust". Gracias a las diversas fases de Fe identificadas y a la presencia de yeso se puede inferir la influencia del derrame en las diversas zonas muestreadas, siendo menor donde la mineralogía no estaba asociada a altas concentraciones de sulfatos. Las fases secundarias de Fe que hay en la zona más cercana al derrame se conocen por su capacidad de incorporación estructural y/o adsorción superficial de EPTs, contribuyendo de esta forma a la inmovilización de la contaminación de metal(oid)es producida por el derrame. Adicionalmente, diversas muestras de otros residuos minero-metalúrgicos fueron analizadas por las mismas tres técnicas, sugiriendo que parte de la mineralogía secundaria de Fe en la zona del derrame ácido de la mina* Buenavista del Cobre *es propia de los procesos comunes que ocurren en ambientes afectados por la minería.*

Palabras clave: fases de Fe; espectroscopía de absorción de rayos-X (XAS); Geoquímica; Cananea; derrame ácido; México.

Escobar-Quiroz, I.N., Villalobos-Peñalosa, M., Pi-Puig, T., Romero, F.M., Aguilar-Carrillo de Albornoz, J., 2019, Identification of jarosite and other major mineral Fe phases in acidic environments affected by mining-metallurgy using X-ray Absorption Spectroscopy: With special emphasis on the August 2014 Cananea acid spill: Revista Mexicana de Ciencias Geológicas, v. 36, núm. 2, p. 229-241.

INTRODUCTION

The mining and metallurgical industry, which produces much of the wealth of modern day society, is a source of contaminated waste material in immense quantities. When underground material from mines is exposed to open air, the change in physicochemical conditions generally alters the chemical forms of potentially toxic elements (PTEs) towards more mobile/bioavailable species. The presence of sulfides (mostly, as pyrite - FeS_2) in mine wastes may generate acid mine drainage (AMD), unless alkaline material is present in the soil disposing matrix. AMD produces severe environmental problems because of the highly acidic conditions generated, which in turn increases considerably the mobility and availability of PTEs.

In addition, concentrated acid is often used expressly by the mining industry to dissolve specific minerals and separate the metal(s) of interest, as it is the case for the Buenavista del Cobre mine in Sonora, in which, after pyrite, quartz and aluminosilicates, the most abundant minerals are those containing copper (Cu). Therefore, the industry has adopted a large field-scale method to spray and leach concentrated sulfuric acid through the Cu- (and Fe-) rich rock piles at the mine. This causes dissolution of these two metals (*cf.* equations 1-3), as well as others contained as impurities in the sulfide mineral matrix, producing highly concentrated acidic sulfate solutions in large quantities, which facilitate subsequently the separation and purification of the Cu metal.

According to Dutrizac (1981) and Watling *et al.* (2009), oxidation of chalcopyrite in sulfuric acid media is expressed as the series of equations 1-3:

$$CuFeS_2 + O_2 + 2H_2SO_4 \rightarrow CuSO_4 + FeSO_4 + 2S^0 + 2H_2O \quad (1)$$

$$4FeSO_4 + O_2 + 2H_2SO_4 \rightarrow 2Fe_2(SO_4)_3 + 2H_2O \quad (2)$$

$$CuFeS_2 + 2Fe_2(SO_4)_3 \rightarrow CuSO_4 + 5FeSO_4 + 2S^0 \quad (3)$$

Large volumes of acid solutions that are leached through the rock piles are confined in dams built downhill from the piles for further processing of the dissolved copper. In August 2014, one confinement dam of the Buenavista del Cobre mine failed, spilling around 40,000 m^3 of acid solution further down into the Sonora river basin (Toscana-Aparicio and Hernández-Canales, 2017). As the acidity of sulfuric acid enriched in dissolved Fe(III) is progressively neutralized, new solid mineral phases are expected to form, ranging from hydroxy-sulfates, such as jarosite [$KFe_3(SO_4)_2(OH)_6$] and schwertmannite [$Fe_8O_8(OH)_6(SO_4)\cdot 10H_2O$], to (hydr)oxides such as ferrihydrite ($5Fe_2O_3\cdot 9H_2O$) and goethite [α-FeO(OH)] at higher pH values (Blowes *et al.*, 1991; Filip *et al.*, 2007; Hayes *et al.*, 2014; Nordstrom *et al.*, 2015). These secondary Fe(III) minerals are of interest in environmental sciences since they play a significant role on the fate of contaminants (Schwertmann and Cornell, 2000) because they are efficient sorbents of organic and inorganic species (Bernstein and Waychunas, 1987; Gerth, 1990; Raven *et al.*, 1998; Schwertmann and Cornell, 2000; Fukushi *et al.*, 2003; Walter *et al.*, 2003; Paktunc *et al.*, 2004; Acero *et al.*, 2006; Filip *et al.*, 2007; Li *et al.*, 2014; Swedlund *et al.*, 2014).

In this work, the EXAFS (extended X-ray absorption fine structure) spectra of different Fe minerals were used as standards in linear combination fits to determine the Fe mineralogy in samples downstream from the acid spill, focusing on detecting the Fe sorbent phases that form under acidic environments. XAS (X-ray absorption spectroscopy) is based on the principle of core electron excitation by X-rays of extremely high intensity. The released photoelectron interacts with the surrounding atoms and provides detailed information of the distances of neighboring atoms, as well as their nature and numbers (Scott, 2013).

In the present study, we identified the major Fe phases that formed from this sulfate-rich spill, and related them to those present in other mining and metallurgical wastes. Since the formation of these Fe minerals follows different kinetic behaviors and depends on different geochemical conditions (in some cases forming metastable, although long-lasting phases, *e.g.*, ferrihydrite), the main goals of this research were (1) to characterize and identify the major Fe phases formed along the Sonora river path, downriver from the spill; (2) to relate them to the physico- and geochemical conditions found around each sample site; and (3) to analyze samples from other mining and metallurgical wastes areas in order to compare the Fe phase speciation across different treatment processes.

MATERIALS AND METHODS

Study areas

The areas studied are located in Mexico, in the northwest (Buenavista del Cobre mine, Cananea; and El Tecolote mine tailings impoundment, Pitiquito; both in the Sonora State); in the north central part (a Zn refinery in San Luis Potosi city); and in the south central part (El Fraile mine tailing impoundment, in Taxco, Guerrero). The sampled points are shown in Figure 1. In the case of the Buenavista del Cobre mine, soils were collected along the dry river bed. The climates of the areas are categorized as semiarid and arid, except for Taxco, which is temperate (INEGI, 2019).

The Buenavista del Cobre mine currently produces Cu from porphyry copper mineralization, which is hosted mainly in volcanic rocks. The lithology of the porphyry inclusion presents quartz-monzonite, monzodiorite, and granodiorite, accompanied by potassic and quartz–sericite alterations and zinc–lead–copper (Zn-Pb-Cu) skarns with strata bound high-grade sulfide and iron-oxide deposits (Meinert, 1982; Ochoa-Landín *et al.*, 2011). As mentioned before, the Cu extraction currently consists of spraying and leaching concentrated sulfuric acid through the Cu-rich rock piles.

In the Taxco mining area the mineralization appears mainly in hydrothermal veins, replacement ores, and stock works hosted in limestone, shale and schist. The flotation treatment plant El Fraile generated tailings that were deposited on calcareous shale. These wastes were deposited in two zones, one of smaller particles (covered with calcareous shale) and another of coarser particles, which is exposed since 1973 (Romero *et al.*, 2007).

El Tecolote tailing impoundment comes from an inactive Cu-Zn-Ag mine. It was a skarn deposit with mineralization of Zn and Cu. In this area the material extracted underground was processed by flotation. The waste generated by this process was deposited directly on calcareous rocks (Cruz-Hernández *et al.*, 2018).

In San Luis Potosi, the study area is limited to the deposition of the solid wastes produced by a Zn electrolytic refinery; these wastes are composed mainly of jarosite, which was synthesized by the metallurgical operations since it takes up Fe and other present elements, and leaves Zn in a dissolved form devoid of other major elements for further purification.

All these other sites were selected for sampling because secondary Fe minerals were detected in previous works (Romero *et al.*, 2007; Cruz-Hernández *et al.*, 2018); therefore, they were considered as good references for comparison with the Buenavista del Cobre mine.

Samples

Nine samples were analyzed in total, including four from the Buenavista del Cobre mine and five from other acidic mine-metallurgical environments. The details are shown in Table 1. Although this

Figure 1. Map showing the study areas and location of samples: a) El Tecolote mine tailings in Pitiquito, Sonora, b) Buenavista del Cobre mine in Cananea, Sonora, c) El Fraile mine tailings in Taxco, Guerrero, and d) Solid hydrometallurgical wastes in San Luis, San Luis Potosi.

Table 1. Location and description of the analyzed samples.

Sample	UTM Coordinates			Locality	Description
	X	Y	Zone		
Ca1[a]	564072	3415176	12	Cananea, Sonora	Contaminated soil very close to the acid spill[b]
Ca2[a]	564026	3414637	12	Cananea, Sonora	Contaminated soil treated with lime, very close to the acid spill[c]
Ca3[a]	563688	3411506	12	Cananea, Sonora	Contaminated soil 10 km from the acid spill
Ca4[a]	565676	3400682	12	Cananea, Sonora	Contaminated soil 20 km from the acid spill
Ta1	433032	2048459	14	Taxco, Guerrero	Superficial oxidized mine tailing
Ta2	432909	2048372	14	Taxco, Guerrero	Oxidized mine tailing
Te	448300	3273662	12	El Tecolote, Sonora	Superficial oxidized mine tailing
SLP1	289779	2453107	14	San Luis Potosi, San Luis Potosi	Solid waste from zinc refinery
SLP2	289751	2453229	14	San Luis Potosi, San Luis Potosi	Solid waste from zinc refinery

[a]Sampling dates: Ca1, Ca2 August 2014; Ca3, Ca4 February 2015. [b]The soil was identified as clearly contaminated by the spill because of its yellow or brown hue and light value as compare to its surroundings, indicating the presence of secondary, newly formed Fe phases. It was taken from the dry river bed and it was put next to the river. [c]Lime treatment: limestone chips and/or lime milk suspension.

number may seem small, beamline work at the synchrotron facility (ALS, Lawrence Berkeley National Laboratory – *cf.* below) for each sample is extremely laborious. We were granted a total of four different sessions consisting of fifteen 8-hour cycles to work at the beamline, which is adequate for obtaining good analytical results. The Buenavista del Cobre mine samples were selected with the following criteria: 1) soil visibly contaminated by the acid spill and confirmed from previous wet-chemical analyses (Ca1 sample); 2) equivalent contaminated soil but treated with lime to neutralize pH (Ca2 sample) and determine this effect on the secondary Fe mineralogy on a very short time-scale; and 3) soil not evidently contaminated, from the same basin, found at 10–20 km distance downriver from the spill (samples Ca3 and Ca4), in order to detect any influence from the spill in the Fe mineralogy. Also, to compare the Fe mineralogy in different acidic mine and metallurgical environments, three samples from other mine tailing impoundments and two samples from hydrometallurgical wastes were processed and analyzed with the same techniques as the samples from the Buenavista del Cobre mine.

The samples were collected by the environmental geochemistry group of the Laboratorio Nacional de Geoquímica y Mineralogía, Instituto de Geología (LANGEM), Universidad Nacional Autónoma de México (UNAM) according to the mexican norm MNX-AA-132-SCFI-2006 (SE, 2006), from the top 5 cm of material; with the exception of Ta2, which was a combined sample of a mine tailings vertical profile collected from 40 to 180 cm in Taxco, Guerrero. The samples were air-dried and passed through a 2-mm round-hole sieve. The pH and E.C. (electrical conductivity) were determined in a 1:5 solid:water ratio following the ISO norm 10390:2005 (ISO, 2005) for the contaminated soils from the Sonora river basin and in a 1:1 ratio in accordance with Thomas (1996) for the samples from the mine tailings. All aqueous solutions were prepared with Milli-Q water (>18.2 MΩ·cm, Millipore). The color of the air-dried soil samples was determined in the laboratory using Munsell soil color charts (Munsell Color, 1975).

Acid digestions and selective sequential extractions (SSEs)

Eleven elements were quantified by a modification of the EPA method 3051a (Environmental Protection Agency; U.S. EPA, 2007). The samples were sieved to 74 μm, 0.5 g of each sample was weighed into a Teflon vessel followed by addition of 9 mL concentrated nitric acid and 3 mL concentrated hydrochloric acid (analytical grade reagents from Sigma-Aldrich). The vessels were placed in the microwave oven (Milestone brand model ETHOS UP) with parameters of 5 min ramp to reach a temperature of 180 °C held for 10 min. After cooling to room temperature, the resulting solution was filtered through Whatman No. 5 filter paper (Whatman International Ltd., Hillsboro, OR) and diluted to 50 mL with Milli-Q water. The resulting solution was additionally filtered with a pore size membrane of 0.05 μm (MF-Millipore membrane). All analyses were performed in duplicate. The solutions were analyzed by ICP-OES (inductively coupled plasma optical emission spectrometry, Perkin Elmer, Optima 8300) at the Instituto de Geología, UNAM. The LoD (limit of detection, μg/L) were: Al (1.2), As (13.6), Ca (9.1), Cd (1.3), Cr (1.1), Cu (1.0), Fe (1.0), Mn (0.9), Ni (1.3), Pb (3.5), Zn (1.5).

The SSEs allow quantification of the labile elements associated with specific solid phases, but also of different major solid constituents (Hayes *et al.*, 2014). The present investigation focused on the Fe phases. Hence, a SSE of three steps was chosen that provides information on the proportion of (1) water-soluble Fe, predominantly as Fe(II) salts, (2) Fe in poorly crystalline phases, and (3) in crystalline phases; these last two items are mainly Fe(III) minerals and in smaller proportion mixed-valence Fe minerals. The following methodology was based on the work published by Drahota *et al.* (2014). Step 1 (soluble Fe phases): 0.4 g of sample was weighed into 50 mL centrifuge tubes, 40 mL of Milli-Q water was added and placed for 10 h in orbital shaking at 200 rpm (in a Lumistell™ AOP-70 stirrer). The suspensions were centrifuged at 4050 g (relative centrifugal force) for 10 min at 20 °C (Centurion Scientific brand PrO-Research centrifuge) and the supernatants were filtered through 0.05 μm membrane filters; these last two steps were repeated at the end of each extraction step. Step 2 (poorly crystalline Fe phases): 40 mL of 0.2 M NH_4-oxalate solution brought to pH 3.0 by 0.2 M oxalic acid (analytical grade reagents by Sigma-Aldrich) was added to the tube with the centrifuged sample at the end of step 1, stirred for 2 h at room temperature at 200 rpm with the tubes covered to keep them in the dark. Step 3 (crystalline Fe phases): the same solution as in step 2 was added to the tube with centrifuged sample at the end of step 2, stirred for 4 h at 80 °C. The filtered samples from step 2 and 3 were diluted with water (ratio 1:3). 10 mL aliquots of each extraction step were taken and 0.5 mL concentrated nitric acid was added to each tube. The solutions were kept in refrigeration until 24 h prior to analysis. The acidified solutions were analyzed by ICP-OES. The LoD (μg/L) for the oxalate matrix analyses were: Al (24), As (132), Ca (196), Cd (17), Cr (17), Cu (25), Fe (55), Mn (23), Ni (20), Pb (57), Zn (30).

Mineralogical analyses

The bulk mineralogy of samples was determined via PXRD (powder X-ray diffraction) using an EMPYREAN diffractometer

equipped with a fine focus Cu tube, Ni filter, and PIXCell3D detector operating at 40 mA and 45 kV at the LANGEM, UNAM. Samples were dispersed with an agate pestle and mortar to <75 μm and mounted in back side Al holders. The analyses were carried out on randomly oriented samples by the step scan method using the measurement range (2θ) of 5° to 70° with an integration time of 40 s and step size of 0.003° at room temperature. Phase identification (and semi-quantification by RIR method) was made using HighScore version 4.5 and Data Viewer version 1.8 software from PANalytical and current PDF-2 and ICSD databases.

The XAS analyses were carried out at the Advanced Light Source (ALS) in Lawrence Berkeley National Laboratory, Berkeley, California, with a beamline 10.3.2 X-ray fluorescence microprobe (Marcus *et al.*, 2004). The EXAFS data were collected in transmission and fluorescence modes, the monochromator used was Si(111) crystal from 2.1 keV to 17 keV. Fe K-edge spectra were collected using a 7-element Ge solid state detector. The X-ray beam size on the sample was 15 μm. The μ-XAS analysis for real samples shows variability between spots; since it is a microfocused technique it allows the analysis of one particle of at least 15 μm. Natural samples are not homogeneous and the analyzed spots were limited by the beamtime availability, limiting in turn the complete identification of Fe phases. Therefore, care must be taken in the interpretation of μ-XAS data and its limitations on the representative nature of the whole sample. The spatial distribution of the elements in the sample was mapped by μ-XRF (X-ray fluorescence). We focused the XAS analysis on spots rich in Fe but also simultaneously containing other PTEs, such as Pb and As, to identify Fe phases that were acting as PTE sequestering minerals. Five to ten scans were collected for each spot. All spectra were calibrated in energy, deadtime corrected (only in fluorescence mode); pre-edge background subtracted, and post-edge normalized and averaged using a suite of custom LabVIEW-based programs available at the beamline. The relative proportions of Fe phases in the samples were determined by LCF (linear combination fitting) of the EXAFS spectra using the Athena software (Ravel and Newville, 2005) performed over the range 2-9 k (where k is wavenumber in $Å^{-1}$) and for XANES (X-ray absorption near edge structure) from 2 to 6 k. Fe-bearing standards include the ones in the XAS database already at the ALS beamline 10.3.2, and those read by the research team in several cycles, mainly (Pb-)As-jarosite (Aguilar-Carrillo *et al.*, 2018). The complete list can be consulted in Table 2, the effectiveness of LCF from collected XAS data depends on the completeness of the database used. The weighting factors were forced to be between 0 and 1; the weighting factor is associated with each standard and quantifies the importance of the standard in reproducing the entire spectral series. This factor prevents a standard to have a negative contribution or to be larger than 1. The sum weights were not constrained in order to make sure that the references were suitable. LCF errors are reported as χ^2, a statistical indicator of "goodness of fit" calculated from the sum of the squared error divided by the degrees of freedom in the fit. The result are presented as the k^3-weighted and normalized Fe K-edge EXAFS spectra, together with the LCF results. In some of the spots chosen the LCF were not satisfactory, most likely because the samples contain other minerals that are not found in the EXAFS database used (Table 2). Consequently, the analysis was restricted to XANES, because this library contains more references. However, only XANES LCF results were reported when there was an improvement. Slight, but significant differences may be found between minerals with different degrees of EPT incorporation or adsorption, such as jarosite with different amounts of As incorporated in their structures or Pb sorbed on them (Aguilar-Carrillo *et al.*, 2018). Another advantage of XAS over XRD is the possibility to identify amorphous or poorly crystalline phases (*e.g.*, schwertmannite and ferrihydrite).

RESULTS AND DISCUSSION

Fe phases in soil samples affected by the Buenavista del Cobre mine acid spill

Ca1 sample (close to the acid spill)

The major Fe phase found by XRD in the Ca1 sample is jarosite (Table 3). High contents of total Fe and Al were detected, as well as low concentrations of Ca and Mn, and much lower concentrations of various PTEs, among which those of Zn and Cu were the highest (Table 4). Most of the Fe is present in crystalline phases, and only 23% as poorly crystalline phases, which is consistent with the major Fe phases found by XRD reported above and by XAS (K-jarosite and an As-jarosite, Table 5 and Figure 2). Also, the yellow hue of the sample (pale yellow, 5Y 8/4) is consistent with the presence of jarosite (Lynn and Pearson, 2000; Schwertmann and Cornell, 2000). The EXAFS LCF indicates that the non-crystalline Fe mineral is schwertmannite, which was also detected as a possible trace mineral by XRD. The pH of 4.1 (Table 3) is expected to show an equilibrium transition zone where the stability shifts from jarosite to schwertmannite (Hayes *et al.*, 2014), therefore, the spectroscopic findings and SSEs are all consistent with each other and with thermodynamic predictions (Bigham *et al.*, 1996). Some As incorporation into jarosite is not rare, although the total As content is relatively low. These finding may be an artifact of the XAS spectral similarities between pure jarosites and As-jarosites (the probable pres-

Table 2. Library used of Fe-bearing standards. (n) = natural sample.

Fe-bearing standard		
EXAFS		
Amorphous ferric arsenate	Hematite (n)	Na-Jarosite
As- Ferrihydrite	Goethite (n)	Pb-Jarosite
As0.07-Jarosite[a]	$GreenRustCO_3$	Pb0.18-As0.14-Jarosite[a]
As0.14-Jarosite[a]	$GreenRustSO_4$	Pb0.16-As0.23-Jarosite[a]
As0.32-Jarosite[a]	K-Jarosite	Pb0.22-As0.40-Jarosite[a]
As0.14-Jarosite-Pb_{sorbed}	K-Jarosite-Pb_{sorbed}	Schwertmannite
As0.32-Jarosite-Pb_{sorbed}	Lepidocrocite (n)	Scorodite (n)
$FeSO_4$	Magnetite	
XANES[b]		
2Line-Ferrihydrite	FeO	Moldavite (n)
Aegirine (n)	Ferrihydrite_2Lines	Montmorillionite_
Akaganeite (n)	Ferrihydrite_6Lines	Na-Montmorillionite_
Andradite (n)	Ferrosilite (n)	Nontronite_ (n)
Augite (n)	Ferrosmectite (n)	Pigeonite (n)
Biotite (n)	FeS_Fluka	Pseudobrookite (n)
Chlorite(Ripidolite) (n)	HydFerrousOxid2LF	Pyrite (n)
Coalingite (n)	Hornblende_ (n)	Richterite (n)
$CoFe_2O_4$	Illite_Smectite (n)	Siderite
Esseneite (n)	Ilmenite (n)	Smectite_ (n)
Fe^{3+}phos	Jarosite_Arizona (n)	Vivianite_Borch (n)
Fe_3O_4 (magnetite)	Jarosite_Spain (n)	Vivianite_Brazil_ (n)
Fe3pyrophosphate	Kaolinite_ (n)	
FeAlginate (n)	Maghemite (n)	

[a]The formulas of the (Pb-)As-jarosites are (Aguilar-Carrillo *et al.*, 2018):
As0.07-jarosite= $(H_3O)_{0.37}Na_{0.07}K_{0.56}Fe_{2.55}(SO_4)_{1.929}(AsO_4)_{0.071}(OH,H_2O)_6$,
As0.14-jarosite= $(H_3O)_{0.35}Na_{0.08}K_{0.57}Fe_{2.77}(SO_4)_{1.86}(AsO_4)_{0.14}(OH,H_2O)_6$,
As0.32-Jarosite= $(H_3O)_{0.40}Na_{0.09}K_{0.51}Fe_{2.90}(SO_4)_{1.68}(AsO_4)_{0.32}(OH,H_2O)_6$,
Pb-As0.14-Jarosite= $(H_3O)_{0.64}Na_{0.18}Pb_{0.18}Fe_{2.59}(SO_4)_{1.86}(AsO_4)_{0.14}(OH,H_2O)_6$,
Pb-As0.23-Jarosite= $(H_3O)_{0.56}Na_{0.28}Pb_{0.16}Fe_{2.62}(SO_4)_{1.77}(AsO_4)_{0.23}(OH,H_2O)_6$,
Pb-As0.40-Jarosite= $(H_3O)_{0.50}Na_{0.28}Pb_{0.22}Fe_{2.49}(SO_4)_{1.60}(AsO_4)_{0.40}(OH,H_2O)_6$.
[b]XANES (X-ray Absorption Near Edge Structure) refers to the XAS energy area closest to the photoelectron leaving the atom, until about 50 eV above this value, called the X-ray absorption edge. The reference compounds used in the EXAFS LCF were also used in LCF of the Fe XANES spectra.

Table 3. Characterization of samples. Abbreviations: Amphibole (Amp), anglesite (Ang), feldspar (Fsp), franklinite (Frk), gypsum (Gp), jarosite (Jrs), kaolinite (Kln), phyllosilicates (Phy), plagioclase (Pl), pyrite (Py), quartz (Qz), smectite (Sme), zeolite (Zeo).

Sample	Dry color Munsell notation	pH	CE (mS/cm)	XRD (%, RIR)
Ca1	Pale yellow 5Y 8/4	4.1	1.801	Qz (52), Phy mica type (24), Kln (11), Jrs (8), Sme (5)[a]
Ca2	Very pale brown 10YR 7/4	6.3	0.953	Pl (47), Qz (45), Zeo (5), Sme (3)[b]
Ca3	Very pale brown 10YR 7/3	ND[c]	ND	Qz (46), Fsp (16), Pl (12), Phy mica type (12), Amp (7), Gp (4), Sme (3)
Ca4	Light yellowish brown 10YR 6/4	5.4	1.022	Pl (52), Zeo (22), Gp (20), Sme (6)
Ta1	Olive yellow 2.5Y 6/8	3.1	2.745	Gp (61), Qz (20), Fsp (12), Jrs (7)
Ta2	Brownish yellow 10YR 6/8	4.1	2.300	Qz (61), Kln (17), Phy mica type (9), Fsp (7), Jrs (4), Gp (2)
Te	Yellowish red 5YR 5/6	4.0	4.985	Gp (42), Qz (21), Fsp (17), Kln (11), Ang (4), Jrs (3), Py (3)
SLP1	Brown – Dark brown 7.5YR 4/4	4.8	19.07	Gp (43), Jrs (38), Frk (18), Qz (1)
SLP2	Dark yellowish brown 10YR 4/6	4.1	21.70	Jrs (53), Gp (29), Frk (16), Qz (3)

[a]Possible traces of pyrite and schwertmannite were identified. [b]Possible trace of hematite. [c]ND: Not determined.

ence of As or Pb in jarosite is not necessarily in the same proportion as in the jarosite standard used, however, the better fits obtained with these PTE-substituted standards may indicate the probable inclusion of these or other PTEs in the spot analyzed).

The PTEs: Cu, Mn, Ni, Cd, and Zn are present in high proportions in water-soluble forms in the sample close to the acid spill (Table 4, step 1); but soluble Fe is also quite high, which has to be in the (II) oxidation state. This means that redox conditions are not completely oxidizing, *i.e.*, probably suboxic conditions prevail at least in certain areas of the soils sampled. This is not surprising considering that in the rainy season these samples are submerged under the running river. The E.C. (1.801 mS/cm) is related to the prevalent metal water-soluble sulfates. This shows that the soil of the Ca1 sample zone is polluted by the sulfuric acid spill, although the water-soluble levels shown are below the limits established by the Mexican regulations (NOM-147-SEMARNAT/SSA1-2004, SEMARNAT, 2007).

Ca2 sample (close to the acid spill, lime added)

The higher pH of 6.3 for this sample is the result of the addition of a mixture of limestone chips and lime milk suspension for remediation purposes. Soluble calcium (Ca) concentrations increased considerably (more than two orders of magnitude, Table 4) due to this lime addition, however, the E.C. value was almost the half of those recorded for Ca1 (0.953 mS/cm, Table 3). This is probably because most of the dissolved Ca is present as a neutral species by complexing with sulfate, phosphate, and dissolved organic matter (Pettit, 2004). Also despite this lime addition, a common brown hue (10YR 7/4, very pale brown) in soils persists (Lynn and Pearson, 2000). No major Fe phase was observed by XRD, except for a possible trace of hematite (Table 3). Al, Ca, and Fe are the major elements found. Total Mn concentration was lower than in the previous sample, but is mostly present in poorly crystalline phases and only a small contribution in water-soluble form. Similarly, the remaining PTEs were found in similar lower concentrations than in Ca1 (Table 4). Fe was detected more evenly distributed between non-crystalline and crystalline phases, the latter in fact surpassing the former, in contrast to the non-neutralized sample. However, again not all Fe quantified in the acid digestion is extractable, indicating an important contribution of non-oxide Fe phases. EXAFS LCF results in three spots show the presence of the non-crystalline phases: schwertmannite and ferrihydrite, but also some scorodite ($FeAsO_4$) and especially carbonate green rust were detected, $[Fe^{II}_{(1-x)}Fe^{III}_{x}(OH)_2]^{x+}\cdot[(x/n)A^{n-}\cdot mH_2O]^{x-}$, where x= Fe^{III}/Fe_{total}, and A^{n-}=interlayer anions with charge *n*. Scorodite contains As(V), but the total concentration of As in the sample was relatively low, and below detection limit in the crystalline phase extraction step. At the given pH of the sample (6.3, Table 3). Ferrihydrite and carbonate green rust stabilities are thermodynamically allowed (Hayes *et al.*, 2014; Schwertmann and Fechter, 1994). Schwertmannite with PTEs in its structure, or in association with silicates, is more stable at near-neutral pH ranges than a PTEs-free schwertmannite (Fukushi *et al.*, 2003), and the time periods for transformation may vary from hours to several years (French *et al.*, 2012). The presence of carbonate green rust is not surprising given the pH increase by the lime addition, but this semi-reduced Fe phase may also form by the seasonal submersion of the soil by the river. Water-soluble concentrations of all PTEs decreased in comparison to the previous sample, as would be expected at higher pH values, although the fraction of extractable Cu in reducible mineral fractions (oxides, step 2) increased (Table 4).

Ca3 sample (10 km downriver from the acid spill)

No major Fe phase was identified by XRD, but major Al and silicates such as quartz, plagioclase, feldspar, micas and also gypsum were detected (Table 3). The latter can be related to the influence of the spill, because no natural gypsum is present in the sampled zone (Ramos-Pérez, 2017). The sample is characterized by a brown hue, a light value, and a middle chroma (10YR 7/3, very pale brown), which is associated with initial to intermediate stages of soil alteration; these hue and value are related to medium to low level conditions of organic matter and combinations of Fe oxides (Lynn and Pearson, 2000). Total Fe was slightly less concentrated than in the previous samples, and occurred mostly in crystalline phases (78%, Table 4). Goethite appears in all three spots analyzed by XAS (Table 5), although only in two of them as a major phase. In the spot where goethite is absent, andradite ($Ca_3Fe_2Si_3O_{12}$) was predominant, a non-oxide phase. Schwertmannite was abundant in spot 1, which could explain the smaller fraction of poorly-crystalline oxides (Table 4). Other Fe phases in lower contents were maghemite (γ-Fe_2O_3), sulfate green rust, and vivianite [$Fe^{2+}Fe^{3+}{}_2(PO_4)_2\cdot 8H_2O$] (Table 5), a phosphate that also contributes to the 22% of non-oxides. The existence of gypsum is consistent with the presence of sulfates in the sample (sulfate green rust). Water-soluble concentrations of PTEs were very low, if detectable at all, even of aluminum (Table 4). The soluble Ca concentration was high, consistent with the presence of gypsum, which is related to residual contamination (Ramos-Pérez, 2017).

Ca4 sample (20 km downriver from the acid spill)

This soil sample has a pH of 5.4 and an E.C. of 1.022 ms/cm (Table 3). Only gypsum, plagioclase, zeolite, and smectite were identified by XRD (Table 3). The total Fe concentration was similar to samples Ca1 and Ca2, and most of it was found in crystalline phases (Table 4), but in contrast to those phases, these oxide phases comprise almost the total Fe measured. Goethite was the predominant phase detected by XAS, as well as some sulfate green rust (Table 5). Concentrations of

Table 4. Results of elemental analyses by ICP-OES (mg/g). Abbreviations: total extracted by sequential extractions (T.S.E.), total extracted by acid digestion (T.A.D.), limit of detection (LoD).

Element		Al	As	Ca	Cd	Cr	Cu	Fe	Mn	Ni	Pb	Zn
Ca1												
Step	1	0.444	<LoD	0.164	0.002	0.001	0.139	0.232	1.673	0.006	<LoD	0.216
	2	1.553	0.075	0.2	<LoD	<LoD	0.043	7.846	0.401	<LoD	<LoD	0.05
	3	2.443	0.024	0.116	0.002	0.004	0.031	25.907	1.124	<LoD	0.006	0.052
T.S.E.		4.44	0.098	0.48	0.004	0.005	0.213	33.985	3.198	0.006	0.006	0.318
T.A.D.		19.745	0.105	1.844	0.008	0.012	0.626	42.117	3.184	0.02	0.041	0.351
Ca2												
Step	1	0.077	<LoD	23.401	<LoD	<LoD	0.006	0.157	0.019	<LoD	<LoD	0.058
	2	2.75	0.072	0.356	0.002	0.002	0.302	16.144	0.426	<LoD	<LoD	0.076
	3	3.84	<LoD	0.116	0.002	0.005	0.142	10.297	0.177	0.009	0.024	0.087
T.S.E.		6.668	0.072	23.873	0.004	0.008	0.45	26.599	0.623	0.009	0.024	0.221
T.A.D.		31.126	0.088	23.46	0.007	0.02	0.562	37.64	0.72	0.024	0.055	0.221
Ca3												
Step	1	0.017	<LoD	5.834	<LoD	<LoD	0.031	0.013	0.217	<LoD	<LoD	0.03
	2	0.729	0.001	0.094	<LoD	<LoD	0.057	2.567	0.646	<LoD	0.027	0.045
	3	1.98	<LoD	0.126	0.003	0.015	0.056	17.382	0.239	0.008	0.04	0.138
T.S.E.		2.725	0.001	6.054	0.003	0.015	0.144	19.963	1.102	0.008	0.068	0.213
T.A.D.		10.735	0.033	6.524	0.005	0.025	0.14	25.616	1.093	0.018	0.089	0.216
Ca4												
Step	1	<LoD	<LoD	41.745	<LoD	<LoD	0.001	0.006	0.041	0.002	<LoD	0.13
	2	1.729	<LoD	0.509	<LoD	0.003	0.091	6.05	0.314	<LoD	0.02	0.047
	3	3.291	<LoD	0.118	0.003	0.023	0.116	22.487	0.193	0.012	0.039	0.108
T.S.E.		5.02	<LoD	42.372	0.003	0.026	0.208	28.543	0.548	0.015	0.059	0.285
T.A.D.		15.143	0.044	41.647	0.005	0.026	0.28	29.103	0.587	0.019	0.067	0.283
Ta1												
Step	1	0.13	<LoD	68.394	0.012	<LoD	0.018	0.028	0.117	<LoD	<LoD	0.253
	2	0.087	0.339	2.982	0.002	<LoD	0.005	13.159	0.033	<LoD	0.204	0.079
	3	0.216	1.925	0.155	0.014	<LoD	0.14	111.263	0.044	0.004	4.961	0.46
T.S.E.		0.434	2.264	71.532	0.028	<LoD	0.163	124.45	0.195	0.004	5.165	0.793
T.A.D.		3.598	2.978	68.244	0.028	0.006	0.227	156.005	0.185	0.004	7.414	0.779
Ta2												
Step	1	0.006	<LoD	3.064	0.001	<LoD	0.007	0.021	0.082	<LoD	<LoD	0.4
	2	0.235	0.268	0.153	0.002	0.002	0.006	9.503	0.04	<LoD	0.219	0.112
	3	1.184	1.151	0.133	0.009	0.008	0.072	67.605	0.144	0.005	2.178	0.81
T.S.E.		1.425	1.42	3.351	0.012	0.01	0.085	77.129	0.267	0.005	2.397	1.322
T.A.D.		9.106	1.672	3.104	0.013	0.023	0.118	78.618	0.333	0.008	2.728	1.28
Te												
Step	1	0.007	<LoD	101.175	<LoD	<LoD	<LoD	0.01	0.008	<LoD	<LoD	0.047
	2	0.789	<LoD	1.467	0.002	<LoD	0.543	10.032	0.07	<LoD	0.031	0.467
	3	1.176	<LoD	0.119	0.009	0.002	1.293	68.825	0.177	<LoD	0.769	0.637
T.S.E.		1.973	<LoD	102.761	0.011	0.002	1.836	78.867	0.255	<LoD	0.8	1.151
T.A.D.		16.784	0.063	102.298	0.082	0.009	5.177	126.508	2.758	0.008	0.784	9.518
SLP1												
Step	1	0.017	<LoD	60.306	7.573	<LoD	3.679	0.006	7.688	0.007	0.359	66.981
	2	0.212	0.483	0.968	0.22	<LoD	0.665	4.012	18.57	<LoD	1.675	3.912
	3	2.533	1.573	0.183	0.579	0.029	4.152	163.633	3.675	0.011	4.868	24.419
T.S.E.		2.762	2.056	61.457	8.373	0.029	8.496	167.651	29.933	0.019	6.903	95.312
T.A.D.		3.077	2.127	61.832	7.966	0.044	8.797	165.165	29.842	0.024	17.308	95.11
SLP2												
Step	1	0.036	<LoD	61.107	7.057	<LoD	3.682	0.008	6.506	0.008	0.393	64.582
	2	0.216	0.483	0.732	0.177	<LoD	0.562	3.907	21.274	<LoD	1.577	3.09
	3	2.597	1.609	0.126	0.566	0.03	4.275	168.08	3.476	0.011	3.752	25.958
T.S.E.		2.849	2.092	61.966	7.8	0.03	8.519	171.995	31.256	0.019	5.722	93.63
T.A.D.		2.847	2.058	62.847	7.712	0.04	8.24	171.09	31.035	0.019	13.597	94.459

Table 5. LCF results of the Fe K-edge k^3-weighted EXAFS.

Sample	Spot	LCF Fe-bearing phase	%[a]	Red. χ^2	Spot	LCF Fe-bearing phase	%	Red. χ^2
Ca1	1	K-Jarosite	86.6	0.149	2	As0.32-Jarosite	92.3	0.897
		Schwertmannite	11.4			K-Jarosite	29.6	
		Total	97.6			Total	121.9	
Ca2	1	As-Ferrihydrite	50.6	2.967	2	Schwertmannite	73.6	0.366
		GreenRustCO3	38.8			As-Ferrihydrite	18.6	
		Total	89.4			Scorodite	9.9	
						Total	102.1	
	3	Schwertmannite	90.4	0.135				
		As-Ferrihydrite	11.8					
		GreenRustCO3	5.9					
		Total	108.1					
Ca3	1 XANES	Goethite	40.5	0.068	2 XANES	Andradite	72.6	0.192
		Schwertmannite	35.1			Goethite	10.2	
		Maghemite	6			GreenRustSO4	8.9	
		Total	81.6			Total	91.7	
	3	Goethite	67.3	1.482				
		Vivianite	14.7					
		Total	82					
Ca4	1	Goethite	47.7	0.157	2	Goethite	48.3	0.165
		As-Ferrihydrite	27.8			As-Ferrihydrite	31.2	
		GreenRustSO4	12.3			GreenRustSO4	9.7	
		Total	87.8			Total	89.2	
Ta1	1	Pb0.18-As0.14-Jarosite	72.8	0.093	2	Pb0.18-As0.14-Jarosite	63.6	0.048
		Goethite				Magnetite	18.8	
		Total	28.5			Goethite	8.5	
			101.3			Total	90	
	3	Hematite	66.3	0.159	4	Magnetite	45.5	0.088
		Goethite	17.2			Pb0.22-As0.40-Jarosite	25.9	
		Schwertmannite	4.2			Goethite	13.2	
		Total	87.7			Total	84.6	
Ta2	1	Goethite	50.6	0.297	2	Goethite	57.7	0.295
		Pb-Jarosite	36.1			As0.14-Jarosite-Pbsorbed	29.7	
		Lepidocrocite	3			GreenRustSO4	5.8	
		Total	89.7			Total	93.2	
	3	FeSO4	40	0.305				
		Goethite	30.9					
		GreenRustSO4	24.9					
		Total	95.8					
Te	1	Goethite	40.5	0.094	2	Goethite	57.3	0.071
		Schwertmannite	39			Schwertmannite	34.2	
		Pb-Jarosite	16.3			GreenRustSO4	16.8	
		Total	95.8			Total	108.3	
SLP1	1	Pb0.18-As0.14-Jarosite	78.5	0.892				
		Scorodite						
		Lepidocrocite	15.8					
		Total	11.7					
			106					
SLP2	1	K-Jarosite-Pb_{sorbed}	75.9	0.364				
		As-Ferrihydrite	32.3					
		Total	108.2					

[a] Molar percent by absorbing atom.

ferrihydrite were also detected in the analyzed spots by XAS, consistent with the 21% of Fe in poorly-crystalline phases. Water-soluble PTEs were quite low (Table 4), and PTEs were evenly distributed between the non-crystalline and crystalline Fe/Mn oxide phases.

General discussion of the samples from the Buenavista del Cobre mine acid spill

It is interesting to note that jarosite was only identified in the Ca1 sample where low pH and most probably high sulfate concentrations are consistent with its formation (Stoffregen, 1993). Although jarosite forms in more acidic environments (around pH 2 to pH 2.5; Li *et al.*, 2014), it may be still present at pH 4.1 because of insufficient time for its transformation, considering the initial pH from the spill was very low (pH 2.2 and 2.3; UNAM, 2016). Jarosite has a large capacity to incorporate both cationic and anionic PTEs in its structure, serving as a natural attenuating mineral under very acidic conditions.

Schwertmannite and ferrihydrite were alternately found in all samples. Both are nanominerals and metastable phases, but ferrihydrite can persist for long time periods in a pH range of 2 to 7.5 (Hayes *et al.*, 2014; Li *et al.*, 2014). Schwertmannite precipitates at slightly higher pH than jarosite, from 2.5 to 4.5 (Walter *et al.*, 2003; Li *et al.*, 2014). Being nanoparticulated, both Fe(III) phases show considerable surface adsorption capacities, and schwertmannite additionally can incorporate oxyanions into its structure. Under semi-arid climate conditions, there is a delay of the metastable phase transformation. Hayes *et al.* (2014) observed ferrihydrite and schwertmannite in mine tailings that have been air-exposed for almost 50 years in IKMHSS (Iron King Mine and Humboldt Smelter Superfund; Dewey-Humboldt, Arizona, USA). On the other hand, Dold and Fontobé (2001) detected schwertmannite in mine tailings in Chile where evaporation exceeds precipitation, probably because in these situations sulfate concentrations are conservative (without leaching effects) and allow stability of this hydroxy-sulfate, provided the pH conditions are also adequate. Another important factor that inhibits their transformation is the presence of high concentrations of different ions or other precipitates incorporated in their structure, for example As(V), or Cr(VI) (Fukushi *et al.*, 2003; Regenspurg and Peiffer, 2005). Schwertmann and Cornell (2000) indicate that crystallization inhibitors (*e.g.* organics and silicate species) stabilize ferrihydrite and retard its transformation to more stable minerals. Swedlund *et al.* (2014) confirmed that arsenate ions stabilize ferrihydrite against transformation to goethite in solutions with pH of 6, 8, and 10. Therefore, since the formation of schwertmannite and ferrihydrite occurs from the gradual neutralization of an acidic solution enriched in PTEs, the incorporation of the latter into the structure or on the surface of these minerals is highly probable and, in consequence, may favor their stabilization.

Some reducing conditions are suggested by the presence of Fe(II)-containing minerals such as vivianite and green rusts, which may be expected under submerged conditions by the running river water during the rainy season. Green rust is produced under reducing conditions and from slightly acidic to slightly alkaline environments, often as an intermediate phase in the formation of Fe oxides (Schwertmann and Fechter, 1994; Abdelmoula *et al.*, 1998). Green rust was identified in the samples with either one of two oxyanions, SO_4^{2-} at pH 4.1 to 5.4, and CO_3^{2-} at pH 6.3, which makes sense if contaminated soils were remediated with lime.

Goethite was identified in samples from the most distal away from the spill, but was absent in samples Ca1 and Ca2 closest to the spill, most probably because the high sulfate concentrations and low pH resulting from the spill select for hydroxy-sulfate minerals such as jarosite and schwertmannite. As sulfate is diluted and/or removed from solution, *e.g.*, by lime additions, the conditions for goethite formation may improve, which is the probable mechanism in samples farthest away from the spill. Goethite is one of the most ubiquitous Fe minerals in soils because it is thermodynamically most stable under humid conditions (Hayes *et al.*, 2014). In addition to its well-known surface adsorption capacity, isomorphic substitutions in goethite are known (Gerth, 1990), which makes this Fe(III) phase a crucial player

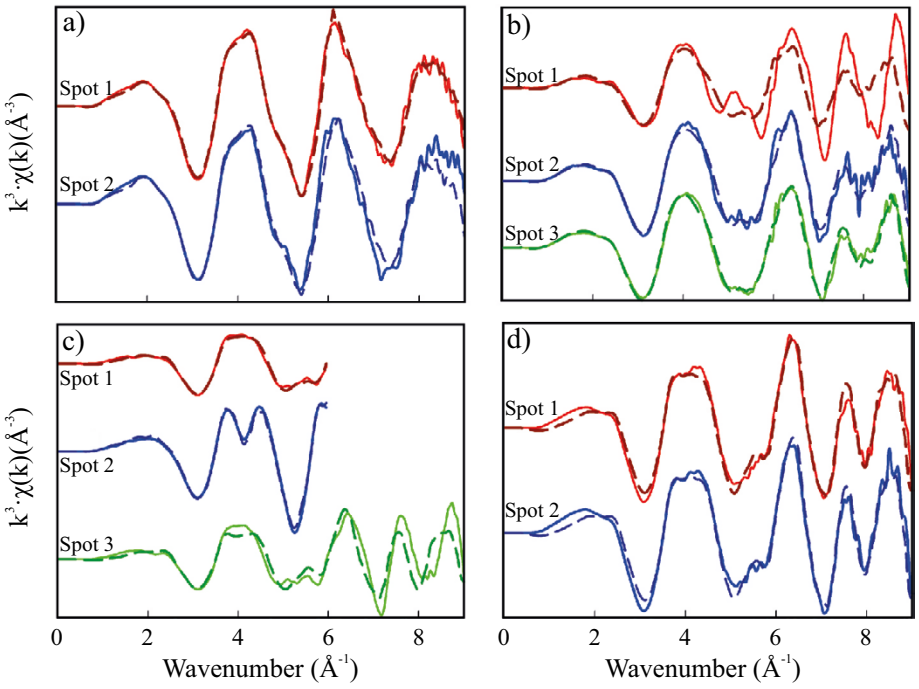

Figure 2. k^3-weighted Fe K-edge EXAFS spectra (solid lines) and LCF (dark dashed lines) of: a) Ca1, b) Ca2, c) Ca3, and d) Ca4.

in the mobility control of ions such as those of PTEs under more circumneutral pH conditions.

Ramos-Pérez (2017) indicated the following mineralogy associated to pristine soils in the study area affected by the acid spill of Buenavista del Cobre mine: quartz, minerals from the mica group (such as muscovite), intermediate members of the plagioclase group (*e.g.*, labradorite), phyllosilicates (as montmorillonite), and some possible trace minerals, such as birnessite (Mn oxide) and hematite. However, hematite was not detected by XRD or EXAFS in our samples Ca1 to Ca4. Also, neither jarosite nor goethite were identified in pristine soil samples. Therefore, their presence is most likely related to the conditions produced by the influence of the acid spill. No ferrihydrite or schwertmannite are expected were identified by XRD in soil samples in the work of Ramos-Pérez (2017), because of their poor crystallinity, but the conditions for schwertmannite precipitation also correspond to the low pH and high sulfate concentrations generated by the acid spill.

Fe phases in other mine tailing and metallurgical samples

Samples Ta1, Ta2 (Taxco, Guerrero), Te (Tecolote, Sonora), SLP1, and SLP2 (San Luis Potosí) showed an acidic pH range from 3.1 to 4.8 (Table 3), and gypsum is present in all sample, which is a sign of acidity and sulfate generation from sulfur oxidation, and proton reactions with calcium carbonates. Gypsum detection by XRD is also confirmed in very high water-soluble Ca concentrations (Table 4). The E.C. values may be imposed mainly by the presence of gypsum (high soluble Ca concentrations, Table 3), with lower aqueous complexation of Ca than in the Buenavista del Cobre mine samples and in minor proportion by metal water-soluble salts (Romero *et al.*, 2008; Murray *et al.*, 2014; Nordstrom *et al.*, 2015; Ramos-Pérez, 2017). The highest E.C. values were those from the solid wastes from the SLP1 and SLP2 zinc processing sites, consistent with the detection of gypsum by XRD and the high quantities of soluble elements (Table 3 and Table 4), especially Zn, which is soluble in the same high order of magnitude as Ca.

The low pH and high sulfate concentration in all these samples lead to jarosite and schwertmannite formation, which is the case for the Buenavista del Cobre mine samples. Both minerals were identified by XAS (Table 5, Figure 3), but only crystalline jarosite was also detected by XRD (Table 3). These minerals are common in AMD and mining environments (Acero *et al.*, 2006; French *et al.*, 2102; Hayes *et al.*, 2014). The yellow hue in the samples might be attributed to jarosite (Lynn and Pearson, 2000). Schwertmannite was not evident in the analyzed spots of sample Ta2. It is noteworthy that in all tailing samples the Fe concentrations quantified in step 3 for crystalline phases considerably surpassed the amount for non-crystalline phases (step 2, Table 4). This fact explains why several known crystalline phases were detected by XAS additionally to jarosite, including goethite, hematite, lepidocrocite, magnetite, and sulfated green rust (Table 5). The latter two with semi-reduced Fe, perhaps in intermediate transformation steps from reduced Fe sulfide to ultimate Fe(III)-containing oxide minerals. It is also notable that no ferrihydrite was detected by XAS, except for SLP2, probably because the low pH and high sulfate concentrations favored schwertmannite formation as the non-crystalline Fe phase (French *et al.*, 2012).

Pyrite was detected in Te sample by XRD, but pyrite spots were avoided in the XAS analysis to better focus on the presence of secondary Fe phases. This justifies that almost 40% of the detected Fe was not an oxide (difference between T.A.D. and T.S.E. Table 4). This is consistent with the primary mineralogy of the El Tecolote tailings for Fe, which includes pyrite, pyrrhotite, and cubanite (Cruz-Hernández *et al.*, 2018). While $FeSO_4$ is the only Fe(II) salt determined by EXAFS LCF in sample Ta2, it should be noted that all samples have a small amount of Fe in the soluble phase (Table 4). Actually, Fe-sulfate salt precipitation by capillary transport in the tailings during the dry season is a well-documented phenomenon (Li *et al.*, 2014; Murray *et al.*, 2014).

Goethite, which can be the responsible for the yellow-brown hue in some mine tailing samples (Lynn and Pearson, 2000; Schwertmann and Cornell, 2000), was not observed in SLP1 and SLP2 samples, probably because these are solid wastes from Zn processing. Jarosite precipitation

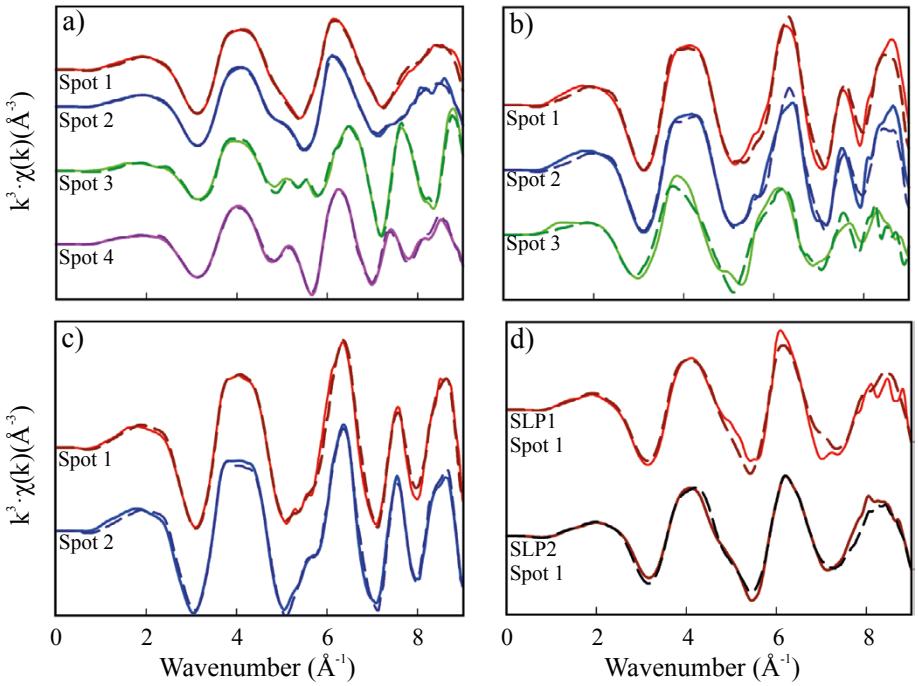

Figure 3. k^3-weighted Fe K-edge EXAFS spectra (solid lines) and LCF (dark dashed lines) of: a) Ta1, b) Ta2, c) Te, and d) SLP1 and SLP2.

is promoted in the Zn refining process, where Fe and other elements are removed as jarosite by precipitation in high sulfate concentration and acidic media, which avoids the formation of goethite (Dutrizac, 1979; Ramos-Azpeitia *et al.*, 2015). Therefore, jarosite was detected by XRD and as predominant phase by XAS in these samples (close to 80%). Franklinite was identified by XRD in samples SLP1 and SLP2, but was not a standard available in the library to include in the LCF of XAS spectra. It constitutes a common secondary mineral in residues from the Zn process (Burke and Kieft, 1972; Zhang *et al.*, 2011; Ramos-Azpeitia *et al.*, 2015), and its presence may be explained by the dark value in the Munsell color determination of the solid wastes (Table 3; Burke and Kieft, 1972). Scorodite was also spotted in sample SLP1 with a pH of 4.8 (Table 3).

Surprisingly, hematite was found in the sample Ta1 with the lowest pH (3.1, Table 3), but it was previously identified in other mine environments at low pH (Bernstein and Waychunas, 1987; Romero and Gutiérrez-Ruíz, 2010) and it was detected in minor quantity as part of the ore in the Taxco zone (Romero *et al.*, 2007). The low abundance of this mineral in the samples might be due to the conditions, because soluble Fe salts, jarosite, and schwertmannite are more prevalent secondary minerals widely found in the unsaturated oxidation zones rich in sulfates and low-water fluxes (Hayes *et al.*, 2014; Li *et al.*, 2014).

Comparison of Fe phases from the acid spill and in mining-metallurgical environments

In the analysis of Fe phases based on pH conditions of the samples from the acid spill, jarosite and schwertmannite were identified at pH 4.1; while at pH 5.4 ferrihydrite, sulfate green rust and goethite were detected. Schwertmannite, ferrihydrite, scorodite, and carbonate green rust were observed at the highest pH of 6.3. Finally, schwertmannite, goethite, maghemite, sulfate green rust, vivianite, and andradite were found in sample Ca3 (unknown pH).

The Fe mineralogy in the mine tailing samples is represented by the jarosite group, specifically in Pb-As-jarosite (Table 5) in the pH range 3.1 to 4.8. Jarosite compounds have the versatility of incorporating a great number of different chemical elements in their structural sites, such as the Fe octahedral position, the S tetrahedral position, and in the coordination cation site, commonly occupied by K (Li *et al.*, 2014). Incorporation of PTEs into the jarosite structure was observed by identifying (plumbo)-arsenical jarosite in different samples (Table 5). Goethite is the second Fe phase found almost ubiquitously in the waste samples. Other minor phases were spotted in these samples, such as sulfate green rust, schwertmannite, ferrihydrite, etc.

The Fe contribution quantified by SSEs of poorly crystalline phases is larger in the acid spill-affected soil samples than in the mine tailing samples and it is consistent with the XAS results (Table 4 and Table 5). These finding is compatible with a fresher formation of these poorly crystalline Fe phases as the acid is neutralized and since of the sampling time was relatively short after the spill event (Table 1). Time is an important factor in the increase of crystallinity of Fe phases in mine tailing samples. The occurring processes are opposite from those in the acid spill, as the pH is gradually decreased by the generation of AMD, and the low pH values and high sulfate concentrations are decisive factors for the increasing stability of jarosite in comparison to schwertmannite and ferrihydrite (Hayes *et al.*, 2014; Schwertmann and Cornell, 2000). Metastable phases can persist over time in the semi-arid climate conditions (Hayes *et al.*, 2014) of the Sonora region. Another factor for the abundance of poorly crystalline phases in the acid spill samples is the existence of crystallization inhibitors in the soil (including organic compounds, phosphates, and silicate species, which are widespread in natural environments). These inhibitors also stabilize metastable Fe(III) minerals (Schwertmann and Cornell, 2000).

CONCLUSIONS

Some of the Fe mineralogy in the samples affected by the acid spill was found by XAS in the form of poorly crystalline phases, such as schwertmannite and ferrihydrite, which are nanominerals with high specific surface areas, and thus potentially immobilizing ionic pollutants through sorption mechanisms. Some minor minerals were also detected (*e.g.*, goethite, jarosites). In the case of jarosite, the conditions of high sulfate concentrations and low pH allowed its formation. Green rust was observed as a carbonate or sulfate compound, the former only in the soil sample that was treated with lime after the spill. Jarosite was the only crystalline Fe mineral in sufficient quantity to be detected by XRD in the samples with grain size <75 μm.

The mineralogical findings are in general consistent with the pH stability range of each mineral. Jarosite is more stable than schwertmannite at low pH and ferrihydrite is more stable than schwertmannite at high pH. This statement is also supported in the mine tailing samples. The pH is one of the factors involved in the precipitation of minerals; time and sulfate concentration are other potential parameters controlling the geochemistry of these minerals.

The type of the jarosite group formed depends on the ions which are present during its formation, and ionic pollutants, such as As(V) and Pb(II) may be immobilized by incorporation into its structure. In the soil and tailings samples K-jarosite, As-jarosite, Pb-jarosite, and Pb-As-jarosite were identified by XAS.

Contamination of samples closest to the acid spill in the Buenavista del Cobre mine was confirmed through the identification of jarosite and schwertmannite, serving as diagnostic minerals to establish an influence of the acid spill on the course of the Sonora river. In the most distal samples from the spill location, the prevailing presence of goethite and ferrihydrite shows a much lower affectation by the sulfuric acid spill, in which the absence of Fe hydroxy-sulfate minerals, such as schwertmannite, suggest sufficient sulfate removal from the system. In mine and metallurgical areas with acidic pH values, in general, similar Fe mineralogies were found like in the areas affected by the sulfuric acid spill in the Buenavista del Cobre mine.

ACKNOWLEDGEMENTS

The first author is thankful to the CONACyT for the Doctoral grant awarded. This work was funded by the Laboratorio Nacional de Geoquímica y Mineralogía, Instituto de Geología (LANGEM, UNAM), We thank to the CONACyT for its financial support provided to the LANGEM, UNAM. We thank Josep Roqué Rosell, Matthew Marcus, and Sirine C. Fakra for their assistance in collecting the XAS data at BL 10.3.2 at the Advanced Light Source (ALS), Lawrence Berkeley National Lab (LBNL). The ALS is supported by the Director, Office of Science, Office of Basic Energy Sciences, U.S. Department of Energy under Contract No. DE-AC02-05CH11231. Thanks are also to lab technicians and students of the Departamento de Geoquímica at the Instituto de Geología, UNAM, for their data of the physicochemical characterization of the contaminated soil samples. We are grateful to Javier Tadeo (Instituto de Geología, UNAM) for technical help in ICP-OES measurements. The authors thank Gabriela Alejandra García Vera for the map design and production. Finally, we acknowledge the editorial work of two anonymous reviewers, who helped considerably in improving the manuscript.

REFERENCES

Abdelmoula, M., Trolard, F., Bourrié, G., Génin, J.M.R., 1998, Evidence for the Fe(II)-Fe(III) Green Rust "Fougerite" Mineral Occurrence in a Hydromorphic Soil and Its Transformation with Depth: Hyperfine Interactions, 112(1-4), 235-238.

Acero, P., Ayora, C., Torrentó, C., Nieto, J.M., 2006, The behavior of trace elements during schwertmannite precipitation and subsequent transformation into goethite and jarosite: Geochimica et Cosmochimica Acta, 70(16), 4130-4139.

Aguilar-Carrillo, J., Villalobos, M., Pi-Puig, T., Escobar-Quiroz, I.N., Romero, F.M., 2018, Synergistic arsenic(V) and lead(II) retention on synthetic jarosite. I. Simultaneous structural incorporation behaviour and mechanism: Environmental Science: Processes & Impacts, 20(2), 354-369.

Bernstein, L.R., Waychunas, G.A., 1987, Germanium crystal chemistry in hematite and goethite from the Apex Mine, Utah, and some new data on germanium in aqueous solution and stottite: Geochimica et Cosmochimica Acta, 51(3), 623-630.

Bigham, J.M., Schwertmann, U., Traina, S.J., Winland, R.L., Wolf, M, 1996, Schwertmannite and the chemical modeling of iron in acid sulfate waters: Geochimica et Cosmochimica Acta, 60(12), 2111-2121.

Blowes, D.W., Reardon, E.J., Jambor, J.J., Cherry, J.A., 1991, The formation and potential importance of cemented layers in inactive sulfide mine tailings: Geochimica et Cosmochimica Acta, 55(4), 965-978.

Burke, E.A.J., Kieft, C., 1972, Franklinite from Långban, Sweden: a new occurrence: Lithos, 5(1), 69-72.

Cruz-Hernández, Y., Ruiz-García, M., Villalobos, M., Romero, F.M., Meza-Figueroa, D., Garrido, F., Hernández-Alvarez, E., Pi-Puig, T., 2018, Fractionation and mobility of thallium in areas impacted by mining-metallurgical activities: Identification of a water-soluble Tl(I) fraction: Environmental Pollution, 237, 154-165.

Dold, B., Fontobé, L., 2001, Element cycling and secondary mineralogy in porphyry copper tailings as a function of climate, primary mineralogy, and mineral processing: Journal of Geochemical Exploration, 74(1-3), 3-55.

Drahota, P., Grösslová, Z., Kindlová, H., 2014, Selectivity assessment of an arsenic sequential extraction procedure for evaluating mobility in mine wastes: Analytica Chimica Acta, 839, 34-43.

Dutrizac, J.E., 1979, The physical chemistry of iron precipitation in the zinc industry. Lead--Zinc--Tin 80', *in* Cigan, J.M., Mackey, T.S., O'Keef, T.J. (eds.) Proceedings of the World Symposium on Metallurgy and Environmental Control: Las Vegas, NV, USA 1980, New York, Cigan, 532-564.

Dutrizac, J.E., 1981, The dissolution of chalcopyrite in ferric sulfate and ferric chloride media: Metallurgical Transactions B, 12(2), 371-378.

Filip, J., Zboril, R., Schneeweiss, O., Zeman, J., Cernik, M., Kvapil, P., Otyepka, M., 2007, Environmental applications of chemically pure natural ferrihydrite: Environmental Science & Technology, 41(12), 4376-4374.

French, R.A., Caraballo, M.A., Kim, B. Rimstidt, J.D., Murayama, M., Hochella Jr., M.F., 2012, The enigmatic iron oxyhydroxysulfate nanomineral schwertmannite: Morphology, structure, and composition: American Mineralogist, 97(8-9), 1469-1482.

Fukushi, K., Sato, T., Yanase N., 2003, Solid-Solution reactions in As(V) sorption by schwertmannita: Environmental Science & Technology, 37(16), 3581-3586.

Gerth, J., 1990, Unit-cell dimensions of pure and trace metal-associated goethites: Geochimica et Cosmochimica Acta, 54(2), 363-371.

Hayes, S.M., Root, R.A., Perdrial, N., Maier, R.M., Chorover, J., 2014, Surficial weathering of iron sulfide mine tailings under semi-arid climate: Geochimica et Cosmochimica Acta, 141(15), 240-257.

INEGI (Instituto Nacional de Estadística, Geografía e Informática), 2019, Climatología (on line), <https://www.inegi.org.mx/temas/mapas/climatologia/> open access, consulted February 3 2019.

ISO (International Organization for Standardization), 2005, ISO 10390:2005, Soil quality. Determination of pH: Geneva, Switzerland, ISO, 7 pp.

Li, J., Kawashima, N., Fan, R., Schumann, R.C., Gerson, A.R., Smart, R.St.C., 2014, Method for distinctive estimation of stored acidity forms in acid mine wastes: Environmental Science & Technology, 48(10), 11445-11452.

Lynn, W.C., Pearson, M.J., 2000, The Color of Soil: Exploring the chemistry of soil color: The Science Teacher, 67(5), 20-23.

Marcus, M.A., MacDowell, A.A., Celestre, R., Manceau, A., Miller, T., Padmore, H.A., Sublett, R.E., 2004, Beamline 10.3.2 at ALS: a hard X-ray microprobe for environmental and materials sciences: Journal of Synchrotron Radiation, 11(3), 239-247.

Meinert, L.D., 1982, Skarn, manto, and breccia pipe formation in sedimentary rocks of the Cananea mining district, Sonora, Mexico: Economic Geology, 77(4), 919-949.

Munsell Color (Firm), 1975, Munsell Soil Color Charts: Baltimore, Maryland, Macheth Division of Kollmorger Corporation, 34 pp.

Murray, J., Kirschbaum, A., Dold, B., Mendes-Guimaraes, E., Pannunzio-Miner, E., 2014, Jarosite versus soluble iron-sulfate formation and their role in acid mine drainage formation at the Pan de Azúcar Mine tailings (Zn-Pb-Ag), NW Argentina: Minerals, vol. 4(2), 477-502.

Nordstrom, D.K, Blowes, D.W., Ptacek, C.J., 2015, Hydrogeochemistry and microbiology of mine drainage: An update: Applied Geochemistry, 57, 3-16.

Ochoa-Landín, L., Pérez-Segura, E., Río-Salas, R., Valencia-Moreno, M., 2011, Depósitos minerales de Sonora, México, *in* Calmus, T. (ed.), Panorama de la geología de Sonora, México: Universidad Nacional Autónoma de México, Instituto de Geología, 299-331.

Paktunc, D., Foster, A., Heald, S., Leflamme, G., 2004, Speciation and characterization of arsenic in gold ore and cyanidation tailings using X-ray absorption spectroscopy: Geochimica et Cosmochimica Acta, 68(5), 969-983.

Pettit, R.E, 2004, Organic matter, humus, humate, humic acid, fulvic acid and humin: Their importance in soil fertility and plant health (on line): CTI Research, <www.humate.info >, consulted February 23, 2019.

Ramos-Azpeitia, H.Y., López-Mata, D.G., Castro-Larragoitia, S.A., 2015, Parámetros de operación en el tratamiento de residuos de jarositas para incrementar la recuperación de Zn: Geomimet, 313, 15-20.

Ramos-Pérez, D., 2017, Evaluación de la contaminación residual y del riesgo ambiental en suelos y sedimentos afectados en la cuenca del río Sonora: Ciudad de México, Universidad Nacional Autónoma de México, Master thesis, 127 pp.

Ravel, B., Newville, M., 2005, ATHENA, ARTEMIS, HEPHAESTUS: data analysis for X-ray absorption spectroscopy using IFEFFIT: Journal of Synchrotron Radiation, 12(4), 537-541.

Raven, K.P., Jain, A., Loeppert, R.H., 1998, Arsenite and arsenate adsorption on ferrihydrite: Kinetics, equilibrium, and adsorption envelopes: Environmental Science & Technology, 32(3), 344-349.

Regenspurg, S., Peiffer, S., 2005, Arsenate and chromate incorporation in schwertmannite: Applied Geochemistry, 20(6), 1226-1239.

Romero, F.M., Gutiérrez-Ruíz, M., 2010, Estudio comparativo de la peligrosidad de jales en dos zonas mineras localizadas en el sur y centro de México: Boletín de la Sociedad Geológica Mexicana, 62(1), 43-53.

Romero, F.M., Armienta, M.A., González-Hernández, G., 2007, Solid-phase control on the mobility of potentially toxic elements in an abandoned lead/zinc mine tailings impoundment, Taxco, México: Applied Geochemistry, 22(1), 109-127.

Romero, F.M., Armienta, M.A., Gutiérrez, M.E., Villaseñor, G., 2008, Factores geológicos y climáticos que determinan la peligrosidad y el impacto ambiental de jales mineros: Revista Internacional de Contaminación Ambiental, 24(2), 43-54.

Schwertmann, U., Fechter, H., 1994, The formation of green rust and its transformation to lepidocrocite: Clay Minerals, 29(1), 87-92.

Schwertmann, U., Cornell, R.M., 2000, Iron oxides in the laboratory. Preparation and characterization: Germany, Wiley-VCH, 188 pp.

Scott, C., 2013, XAFS in a Nutshell, in Taylor and Francis (eds.), XAFS for everyone: Florida, CRC Press, 3-30.

Secretaria de Economía (SE), 2006, Norma Oficial Mexicana MNX-AA-132-SCFI-2006, Muestreo de suelos para la identificación y la cuantificación de metales y metaloides, y manejo de la muestra: Secretaria de Economía, Diario Oficial de la Federación, 29 pp.

SEMARNAT (Secretaría de Medio Ambiente y Recursos Naturales y Pesca), 2007, NORMA Oficial Mexicana NOM-147-SEMARNAT/SSA1-2004: Mexico, Diario Oficial de la Federación, México, 69 pp.

Stoffregen, R. E., 1993, Stability relations of jarosite and natrojarosite at 150-250 °C: Geochimica et Cosmochimica Acta, 57(11), 2417-2429.

Swedlund, P.J., Holtkamp, H., Song, Y., Daughney, C.J., 2014, Arsenate-

ferrihydrite systems from minutes to months: A macroscopic and IR spectroscopic study of an elusive equilibrium: Environmental Science & Technology, 48(5), 2759-2765.

Thomas, G.W., 1996, Soil pH and Soil Acidity, *in* Sparks, D.L., Page, A.L., Helmke, P.A., Loeppert, R.H. (eds.), Methods of Soil Analysis Part 3—Chemical Methods, SSSA Book Series 5.3: Madison, Soil Science Society of America, Inc. and American Society of Agronomy, Inc., 475-490.

Toscana-Aparicio, A., Hernández-Canales, P.J., 2017, Gestión de riesgos y desastres socioambientales. El caso de la mina Buenavista del Cobre de Cananea: Investigaciones Geográficas, 93, 1-14.

UNAM (Universidad Nacional Autónoma de México), 2016, Informe final de la UNAM, Informe final, Diagnóstico ambiental en la cuenca del río Sonora afectada por el derrame del represo "Tinajas 1" de la mina Buenavista del Cobre, Cananea, Sonora, on line, <http://www.fideicomisoriosonora.gob.mx/apoyos_DiagnAmbientalUNAM.html> open access, consulted February 3 2019.

U.S. EPA (United States, Environmental Protection Agency), 2007, Method 3051A (SW-846): Microwave assisted acid digestion of sediments, sludges, soils, and oils: Washington DC, EPA, 30 pp.

Walter, M., Arnold, T., Reich, T. y Bernhard, G., 2003, Sorption of uranium(VI) onto ferric oxides in sulfate-rich acid waters: Environmental Science & Technology, 37(13), 2898-2904.

Watling, H.R., Elliot, A.D., Maley, M., van Brownswijk, W., Hunter, C., 2009, Leaching of a low-grade, copper–nickel sulfide ore. 1. Key parameters impacting on Cu recovery during column bioleaching: Hydrometallurgy, 97(3-4), 204-212.

Zhang, Y., Yu, X., Li, X., 2011, Zinc recovery from franklinite by sulphation roasting: Hydrometallurgy, 109(3-4), 211-214.

Manuscript received: july 23, 2018
Corrected manuscript received: march 10, 2019
Manuscript accepted: march 14, 2019